Journal of Magnetism and Magnetic Materials 540 (2021) 168451

Effects of magnetic-elastic anisotropy on magnetoelectric gyrator with ferrite/PZT/ferrite laminate for enhancement of power conversion efficiencies

Jitao Zhang1[†], Kang Li¹, Qingfang Zhang¹, D. A. Filippov², Jie Wu¹, Jiagui Tao³, Jing Chen³, Liying Jiang¹, Lingzhi Cao¹ and Gopalan Srinivasan⁴

1College of Electrical and Information Engineering, Zhengzhou University of Light Industry, Zhengzhou 450002, China

2Institute of Electronic and Information Systems, Novgorod State University, Veliky Novgorod 173003, Russia

3State Grid of Jiangsu Electric Power Co., Ltd. Nanjing 210024, China

4Physics Department, Oakland University, Rochester, Michigan 48309, USA

ABSTRACT

Effects of magnetic-elastic anisotropy on ferrite/lead zirconate titanate (PZT)/ferrite magnetoelectric (ME) gyrators were investigated for power conversion efficiency further improvement, and a methodology was introduced by changing the direction of applied magnetic field (H_{DC}). Simulation by using finite element method provides a clear evolution of magnetic flux density distribution in ferrite as H_{DC} rotates. Consequently, enhanced ME coupling as well as power conversion efficiency (PE) was achieved under a certain angle with maximum effective magnetic field applied especially at intensive magnetic fields. Experimental results show that current (I)-voltage (V) versus directional angle (θ) between H_{DC} direction and longitudinal direction of ME sample and PE vs θ data can essentially track the dynamic piezomagnetic coefficient (DPMC) vs θ profile, indicating that the H_{DC} rotation induced anisotropic magneto-elastic variations are responsible for the eventual PE improvement. For higher H_{DC} =980e, PE reaches its maximum of 76.5% at θ =75° relative to its counterpart of 47.6% at θ =0°, exhibiting an approximately 1.69 times higher enhancement. Therefore, the feasibility of an efficient approach was verified by the obtained results, providing possibilities for PE further improvement and enhanced flexibilities for ME gyrator design.

I. Introduction

An ideal non-reciprocal electronic device prototype of gyrator with passive, linear and lossless merits was conjectured by Tellegen based on transduction of magnetic

1

[†] Corresponding author: Tel. /Fax: +86 371 86601601. E-mail address: zhangjitao@zzuli.edu.cn (J. T. Zhang)

flux and electric charge in 1948, which was recognized as the fifth missing fundamental component circuit with two-port four-wire configuration[1]. Capacitor-to-inductor mutation function accomplished by an ideal gyrator terminated with a capacitor behaves like an inductor, which is useful for the design of inductor filters[2, 3]. In the last decades, the research revival of magnetoelectric (ME) has propelled the gyrator realization to move forward, and ME-coil configuration can fulfill the requirements of gyrator basic constraints[4]. In ME gyrators, the power transfer of ME gyrator is from electric to magnetic energies via the coil or vice versa, and then the magnetic field was converted to elastic strain due to magnetostrictive effect, and finally a conversion from the elastic strain to electric through piezoelectricity[5, 6]. Therefore, concrete evidence has been provided that the ME composite plays a vital role in gyrator scheme involving magnetic and electric mutation conversions, whereby significant ME couplings mediated by strain between magnetostrictive and piezoelectric phase under external magnetic/electric field application [7, 8]. In this case, flourishing research on controlling and improving elastic strain coupling of voltage (V)-current (I)/I-V ME gyrators are actively conducted[9-11]. Pioneer work of ME gyrator was proposed by Dong et al. in 2006, taking advantage of magnetic-elastic/elastic-electric conversion a theoretical estimation of I-V conversion coefficient up to 2500V/A in the vicinity of resonance was predicted by equivalent circuit method[12, 13]. Nevertheless, the research on ME gyrator was stagnant in the following years, since effective approaches on improving the weak ME coupling induced by magnetic-elastic conversion are extremely scarce. A surge revival of ME gyrator studies emerged in 2016, and studies were focused on ones with enhanced stability and power conversion efficiency (PE) implemented by improving magnetic-strain conversion via structural and parametric optimizations [14-16]. In 2017, Leung et al. reported the influence of topical optimum parameters including thickness ratio n, load resistance R_L and magnitude of bias field H_{DC} on PE in layered ME laminates, and the enhanced magnetic-strain conversion of the NZFO ferrite layer was employed to explain the increased power drive in ME gyrators[17, 18]. Moreover, the progress in ME gyrator has been advanced to aim at magneto-elastic strain couplings then PE enhancement by means of rare earth doping in spinel ferrites, and built-in magnetization grading induced by various ion doping on magnetostrictive materials lead to stronger magnetic-elastic conversion and then generate to higher PE at optimum magnitude of H_{DC} under low input[19-21]. Very recently, versatile methodologies including high mechanical quality factor (Q) materials selection, minimizing geometrical demagnetization effect and different polarized/magnetized schemes have successively been reported for improving PE and reducing power consumption in ME gyrators, and the experiment results show that the enhanced magneto-elastic strain coupling by using high Q material is responsible for achievable higher PE at optimum bias[22-24]. Efforts so far have primarily focused on improving isotropic dynamic magneto-elastic strain to further enhance PE in ME gyrator[25]. However, actually the ME coupling can also be effectively improved by the anisotropic dynamic magneto-elastic strain caused via altering direction of H_{DC} , thereby reducing energy loss in magneto-elastic-electric conversion.

Therefore, research on the impact of anisotropic magneto-elastic strain seems necessary for PE improvement in ME gyrators, anticipating achievable higher PE and reduced power dissipation in ME gyrator.

In this work, an effective approach is proposed to enhance PE in ME-coil gyrators consisting of tri-layer ferrite/PZT-8/ferrite with anisotropic magneto-elastic strain induced by H_{DC} direction. Compared with the previous reports, endeavors have contributed to improving the magneto-elastic-electric conversion in the power transfer process. Anisotropic magneto-elastic strain induced by changing $H_{\rm DC}$ direction was systemically investigated, and the optimal H_{DC} direction was found to transfer more vibrating energy at the resonance condition, thereby mitigating the energy dissipation in the magneto-elastic-electric conversion process. In this case, the dynamic anisotropic magneto-elastic behaviors in magnetostrictive phase were characterized under various H_{DC} vectors, followed by the characterizations of ME gyrator including I-V conversion ratios, inductance-capacitance conversion characteristics and PE under various H_{DC} vectors. Optimum direction of H_{DC} existed as expected to increase the PE under extremely low input power density, especially in intensive magnetic field. Therefore, certain non-zero H_{DC} directional angle might facilitate magneto-elastic-electric energy transfer efficiency due to the anisotropic magneto-elastic behaviors of spinel ferrites.

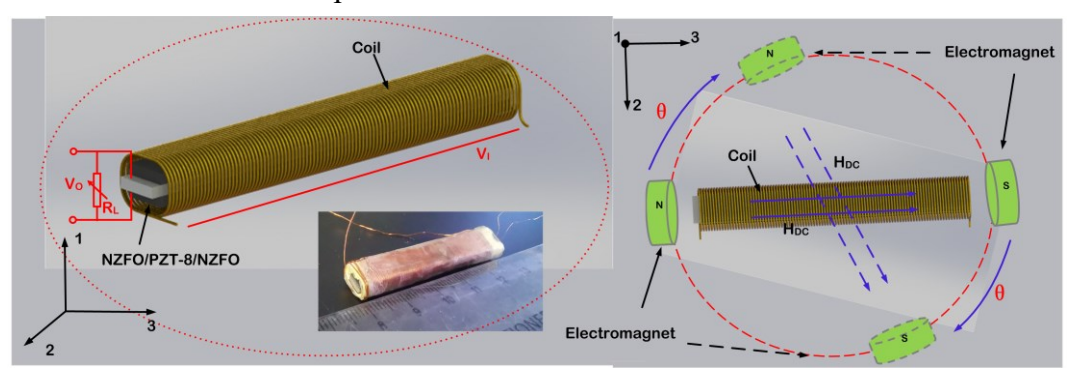


Fig.1. Schematic diagram, photograph and the experimental scheme of the presented ME gyrator.

II. Experiments

Polycrystalline nickel zinc ferrite with composition of Ni_{0.8}Zn_{0.2}Fe₂O₄ (NZFO) from starting powders of ZnO, NiO and Fe₂O₃ in compliance with its mole ratio was synthesized via conventional solid-phase sintering methods, and specific details were documented in our previously reported literature[26]. Sintered bulk NZFO block was cut into thin pieces with dimensions of 23mm×5mm×0.5mm by a low-frequency diamond saw. Figure 2 shows the X-ray diffraction spectrum (XRD) of NZFO polycrystalline platelets, and the indexing of the reflection maxima (peaks) was conducted successfully. The emerging positions of (111), (220), (311), (222), (400), (422), (511), (440) and relative intensities for all the diffraction peaks match well with the standard XRD pattern of Fe₃O₄ (PDF No.75-0449), revealing favorable faultless crystallization and spinel structure [27, 28]. The tri-layered ME composite consists of NZFO platelet and piezoelectric ceramic of PZT-8 slab (purchased from

Bailing Electronic Ceramics Co., Ltd. Zibo, China), with dimensions of 25 mm×5 mm $\times 0.5$ mm, was fabricated by epoxy adhesive. For the influences of H_{DC} direction on magneto-elastic-electric conversion characterization, the AC magnetic field (H_{AC}) generated from a solenoid was powered by an AC/DC current source (Keithley Model 6221), and the ME structure centered in the solenoid and its longitudinal direction coincided with H_{AC} . A static magnetic field H_{DC} , with variable direction supplied by an electromagnet (Eastchanging Model EM3) fixed in rotary base and monitored by a gaussmeter, and a directional angle (θ) between H_{DC} direction and longitudinal direction of ME sample can be obtained from the calibrated scale. The schematic diagram, photograph and the experimental scheme of the presented ME gyrator were illustrated in Fig. 1. Measurements of dynamic magneto-elastic responses were carried out by an optical non-contact measurement system with laser Doppler vibrometer (Polytec Model OFV-5000/505). Gyrator effects of capacitance, inductance and impedance mutation conversion were measured by an impedance analyzer (Keysight Model E4990A). Furthermore, the input power (P_i) of the ME gyrator was provided by a function generator (Tektronix Model AFG3021B) and an amplifier (Ametek Model 5113), and a load resistor R_i of 1 Ω was serially connected into the input loop for input current (I_i) monitoring $(P_i=i^2R_i)$. A variable load resistor (R) was directly connected to the PZT slice for output power (P_0) calculation $(P_o=U^2/R)$, and then PE can be calculated by the ratio of P_o and P_i .

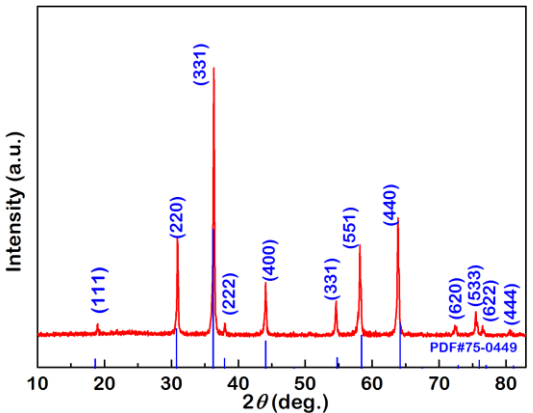


Fig. 2. XRD patterns of NZFO sample at room temperature with standard one of Fe₃O₄ for comparison

III. Results and discussions

Magnetostrictive layer in ME composites serving as the actuating layer will produce a magnetic-elastic conversion once the ME sample is subjected to a magnetic field. Accordingly, the magnetic properties of magnetostrictive phase are significant to evaluate the performance of magneto-elastic-electric power conversion in ME gyrator, especially in the variations of H_{DC} vector. A small sample to be tested with dimensions of 5mm×1mm×1mm was cut from the NZFO platelet, and its magnetic properties were measured by using a vibrating sample magnetometer (VSM) to obtain the typical magnetization hysteresis loops for the longitudinal and transversal directions, respectively. As illustrated in Fig 3, an obvious discrepancy in magnetization process could be clearly observed in the longitudinal and transversal

directions of NZFO platelet due to the different sized-induced demagnetization field. The magnetization value (M) of longitudinal direction of NZFO is higher than that of its transversal direction, whereas the opposite trend is found when H is over ~890 Oe. This discrepancy in magnetic properties is mainly attributed to the variations demagnetization field caused by the H_{DC} rotations, resulting in easy-magnetized axis along longitudinal direction with respect to the rectangular ME samples[29]. In addition, the remnant magnetization (M_r) for the longitudinal and transversal directions of NZFO sample was found to be approximately 1.97emu/g and 0.32emu/g respectively, and the coercive fields (H_c) were 20Oe and 10Oe respectively.

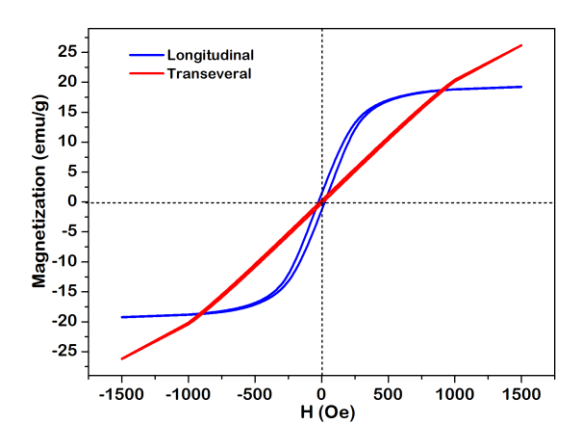


Fig.3 Magnetic hysteresis loops for the longitudinal and transversal directions of NZFO sample

The magnetic field distribution inside the ME composite with dimensions of 25mm×5mm×1mm was evaluated by the finite element method. The ME composite is immersed in a huge enough air providing a natural environment to avoid the influences of magnetic field distribution around the sample[30]. Simulations were carried out under the magnitudes of H_{DC} fixed at 30Oe and 100Oe, respectively, and simultaneously ME composite rotates 30° each time along its central axis within the range of 0° -90°. Results show the magnetic flux density distributions in x-y plane of magnetostrictive phase as illustrated in Fig. 4(a)-(h). Inhomogeneous distribution of the magnetic flux density with maximum occurring at center regions can be clearly observed due to edge effects and demagnetization effects [31, 32]. As θ is increased from 0° to 90° with increment of 30°, the edge effect becomes appreciable and then the maximum magnetic flux density decreases from 5×10⁻²T to 1.2×10⁻²T at 30Oe. By contrast, flux density for ME composite exhibits much higher under 100Oe and corresponding maximum drops from 0.16T to 0.05T. From the simulation results obtained above, there is a significant attenuation in magnetization with θ rotations and an approximately one order of magnitude enhancement with applied magnetic field increased to 1000e. Furthermore, we infer from the results that the variations in magnetization will directly affect the dynamic magneto-elastic couplings and lead to anisotropic dynamic magneto-elastic response. To describe that, anisotropic dynamic magneto-elastic characterizations will be implemented as follows.

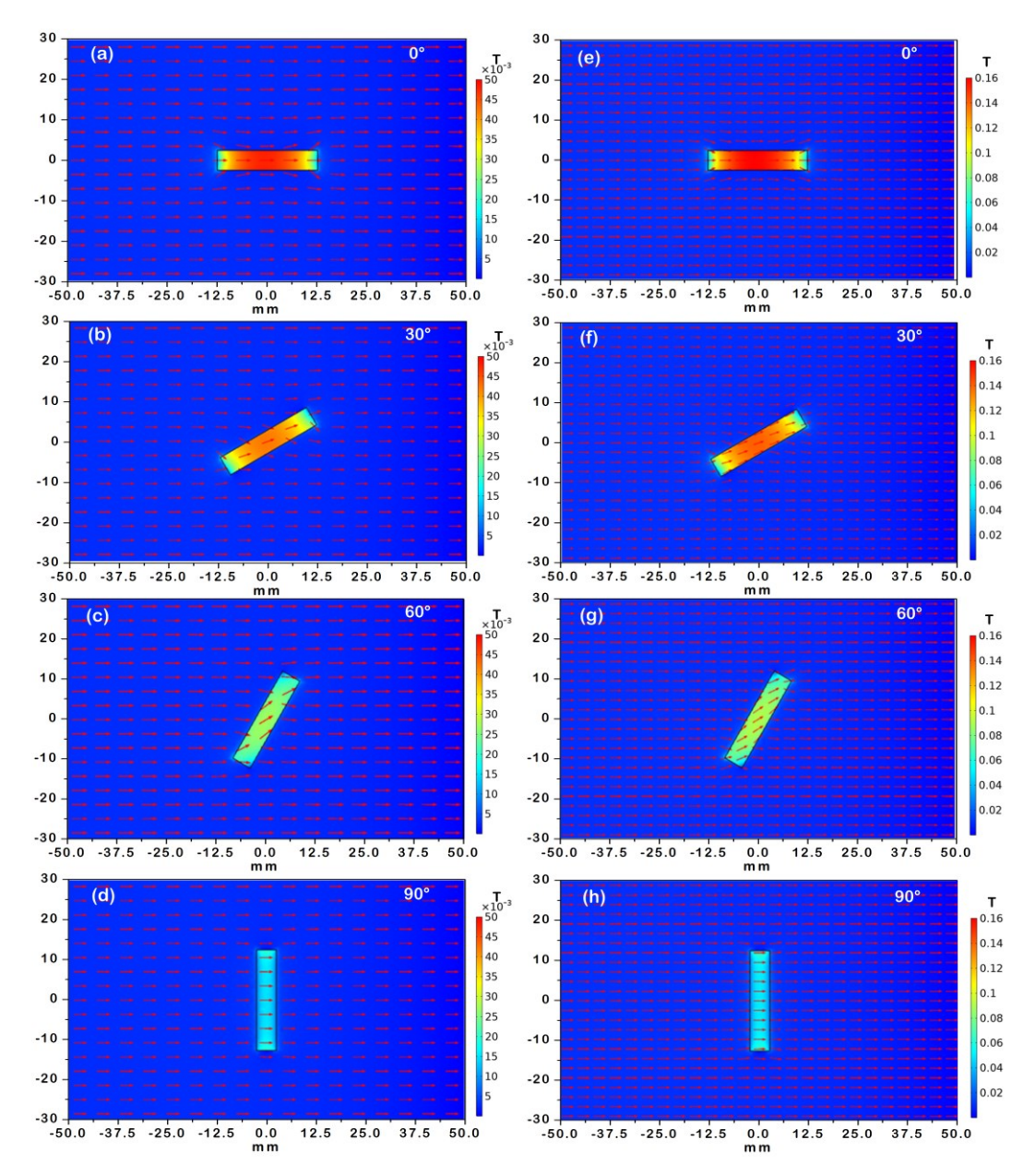


Fig.4. Magnetic flux density distributions in x-y plane of NZFO at H_{DC} =30 Oe for θ = (a) 0° (b) 30° (c) 60° (d) 90° and at H_{DC} =100 Oe for θ = (e) 0° (f) 30° (g) 60° (h) 90°.

For the purpose of revealing the dynamic magneto-elastic conversion process of ME gyrators under different H_{DC} conditions, the dynamic piezomagnetic coefficient (DPMC), regarded as real-time dynamic magnetostrictive responses to AC magnetic field with amplitude of 1Oe, was measured in the longitudinal direction of NZFO platelet by non-contact optical method and more details about the measurements can be found in previously reported literature[33, 34]. The anisotropic DPMC under various H_{DC} can be calculated by the formula of[28]

$$d_{3\theta} = 2\lambda_{3\theta}/lH_{AC}, \tag{1}$$

where $\lambda_{3\theta}$ is the dynamic vibration displacement of the longitudinal direction under various θ , l represents the length of the sample, and H_{AC} denotes the AC magnetic field. Figure 5 illustrates the frequency f dependence of DPMC in the vicinity of

resonance. All peaks of the DPMC spectrum occurred at exact resonance frequency of 100.3kHz, but the magnitude demonstrates anisotropic behaviors along θ . Specifically, for H_{DC} =23Oe, the maximum of 22.35ppm/Oe in DPMC at resonance continuously decreases to its minimum of 11.37ppm/Oe with θ increased from 0 to 90°, as shown in Fig 5(a). As the applied field H_{DC} increased to 46Oe, amplitude of DPMC has an overall slight improvement for all θ as shown in Fig. 5(b), maximum of 23.41ppm/Oe and minimum of 13.12ppm/Oe correspond to 0° and 90°, respectively. Nevertheless, the linear growth in DPMC peak versus θ is broken when H_{DC} =980e, the DPMC peak shows an initial increase from 9.13ppm/Oe at θ =0° and reaches its maximum of 21.6 ppm/Oe at exact θ =75°, and then displays a moderate decline to 11.83ppm/Oe as θ is increased to 90°. Similarly variations can be observed under H_{DC} =149 Oe, and all curves have a decrease relative to H_{DC} =149 Oe (as shown in Fig. 5(d)). As a consequence, anisotropic DMPCs behaviors were activated by various applied θ , and the emerging point of θ for maximum DMPC varied with applied magnetic field. Therefore, the angles θ for approaching maximum DPMC under lower and saturation fields are 0° and 75°, respectively. Resonance DPMC could be further improved by this operation effectively, anticipating much stronger magneto-elastic-electric conversion will be reached in ME gyrators.

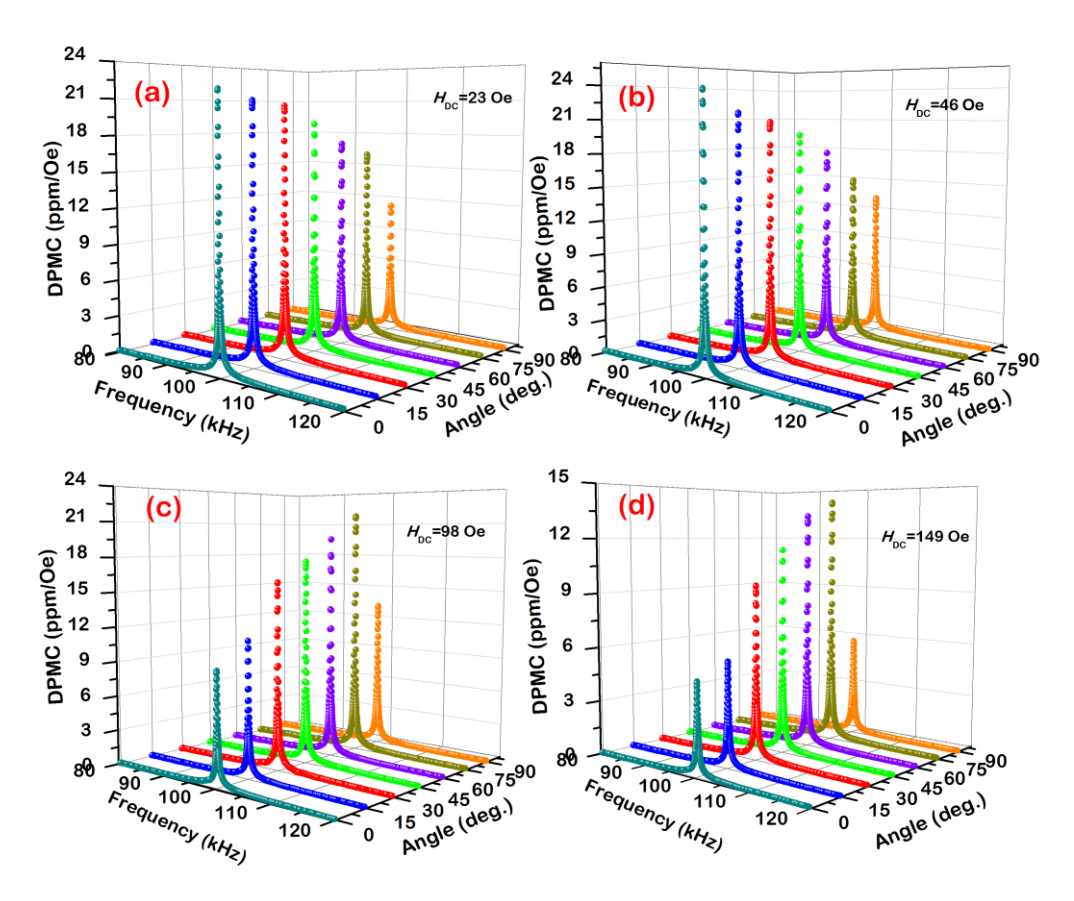


Fig 5. DPMC spectrum around resonance for θ varied from 0° to 90° under (a) H_{DC} =23 Oe; (b) H_{DC} =46 Oe; (c) H_{DC} =98 Oe; H_{DC} =149 Oe.

To further clarify the influences of θ on DPMC, the resonance DPMC peaks for various θ were measured in the range of 0° and 360° under several representative H_{DC} , as illustrated in Fig 6.Resonance DPMC vs θ profile for 23Oe and 46Oe show typical twofold symmetry in the polar coordinate diagram, whereas 'butterfly-like' fourfold symmetry in the polar coordinate diagrams were observed in 980e and 1490e. Coincidentally, the occurring optimum θ for achievable maximum DPMC seems identical for lower and saturation field, respectively. Namely, maximum resonance DPMC occurred at θ =0° and 180° under lower field of 23Oe and 46Oe, while the one shifted to θ =75°, 105°, 255°, and 285° once the applied field exceeded 460e. For H_{DC} =98Oe, the DMPC reaches its maximum of 21.6ppm/Oe at θ =75° compared with counterpart of 9.37ppm/Oe at θ =0°, and thus an approximately 2.30 times enhancement can be obtained. The cause of anisotropic DPMC is the mutual effect of intrinsic parameters, which is quite a complex process [35]. As H_{DC} rotates in the range of 0° to 360° under lower magnetic field, the direction of magnetization nearly attains constant in the direction of longitudinal and then the demagnetization field can be ignored due to the non-180° magnetic domain switches[36]. Nevertheless, the situation seems more complex once $H_{\rm DC}$ reaches its saturation state. In this case, Zeeman energy and demagnetization energy varied by H_{DC} rotations, and then the total energies including magnetic anisotropy energy, exchange energy, demagnetizing energy and magneto-elastic energy approaches the minimum Gibbs free energy[37, 38]. In this case, the demagnetization field (H') should be considered and can be estimated by H=-NM, where N represents demagnetization factor. The effective magnetic field H can be described as $H=H_{DC}-H'$. According to coordinate system, effective magnetic field H with θ rotations can be described as

$$\begin{cases} H_1 = 0 \\ H_2 = H \sin \theta , \\ H_3 = H \cos \theta \end{cases}$$
 (2)

where $H_i(i=1,2,3)$ represent three mutual orthogonal components with its expression of $H(\theta) = \sqrt{H_2^2 + H_3^2}$. Note that demagnetization field H' of the transversal direction of the ferric sample is much higher than that of longitudinal direction, the H_2 is too weak to be ignored. As such, the θ dependence of DPMC (d) can be calculated as[28]

$$d(\theta) = \frac{\partial \varepsilon}{\partial H_{DC}} = 2\lambda_s \left[\coth(\eta H \cos \theta) - \frac{1}{\eta H \cos \theta} \right] \times \left\{ \eta \left[1 - \coth(\eta H \cos \theta)^2 \right] - \frac{1}{\eta (H \cos \theta)^2} \right\}$$
(3)

where $\eta=3\chi_{\rm m}/M_{\rm s}$, ε represents strain of ferrites, $\lambda_{\rm s}$ is the saturation magnetostriction of ferrites, $\chi_{\rm m}$ and $M_{\rm s}$ are initial magnetic susceptibility and saturation magnetization, respectively. From Eq.3, assuming that there is an optimum $H_{\rm DC}$ defined as $H_{\rm o}$. When the longitudinal component of effective magnetic field $H\cos 0 \le H_{\rm o}$, DPMC shows a decrease with θ increased from 0° to 90°. While for $H\cos 0 > H_{\rm o}$, the $H\cos \theta$ becomes uncertain. That is why the DPMC travels a climb and then fall tendency with θ increased from the range of 0° to 90° once $H_{\rm DC}$ is higher than 46Oe, and then the optimum θ appeared at 75° was determined by magnetization and demagnetization field. Therefore, the magnitude of $H_{\rm DC}$ as well as the θ determines the DPMC

anisotropic behaviors, and optimum DPMC can be acquired by adjusting appropriate angles.

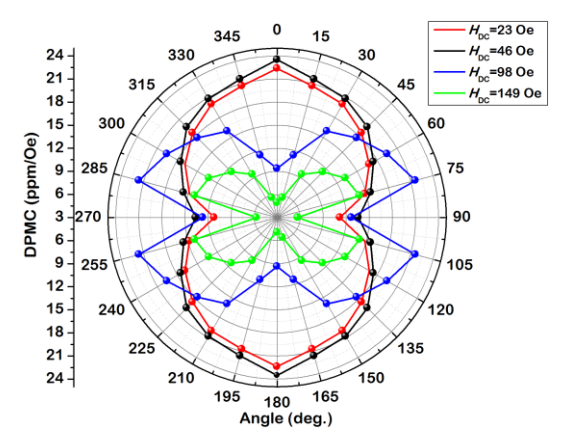


Fig 6. Polar diagram for resonance DPMC as a function of θ in the range of 0°-360° under H_{DC} =23, 46, 98 and 149 Oe, respectively

I-V conversion ratio is a significant indicator to reflect the capability of gyration effects, representing non-reciprocal conversions in the two ports from input current of coil to output voltage of piezoelectric layer. A set of I-V conversion ratio curves at resonance were characterized with θ rotations under various typical field applications. The response clearly increases with frequency and reaches its maximum ratio at their resonance of 89.6 kHz, as shown in Fig 7. For H_{DC} =230e, peak values of I-Vconversion ratio decrease from 1199.1V/A to 382.8V/A corresponding the θ increased from 0° to 90°, as illustrated in Fig 7(a). Similar variations but enhanced amplitude were also obtained in Fig 7(b) for H_{DC} =46Oe, and its maximum and minimum are 1371.2V/A and 549V/A at 0° and 90°, respectively. Therefore, I-V conversion ratio reaches its maximum at lower field when the direction of H_{DC} is parallel to the longitudinal of ME sample (θ =0° or 90°). As the H_{DC} is further increased to a higher field of 98 Oe, the I-V resonance peak initially increases and then decreases with θ , a maximum of 1167.9V/A at θ =75° can be obtained as illustrated in Fig.7(c), showing 1.67 times higher than that of 0° under lower magnetic field. Similarly, for $H_{\rm DC}$ =149Oe, identical tendency in Fig. 7(d) can be observed with slight amplitudes on the ratios. We found that the DMPC vs θ profiles can essentially track I-V vs θ profiles under various lower and higher magnetic fields, which means the variations of magneto-elastic strain are responsible for the obtained results of *I-V* ratios.

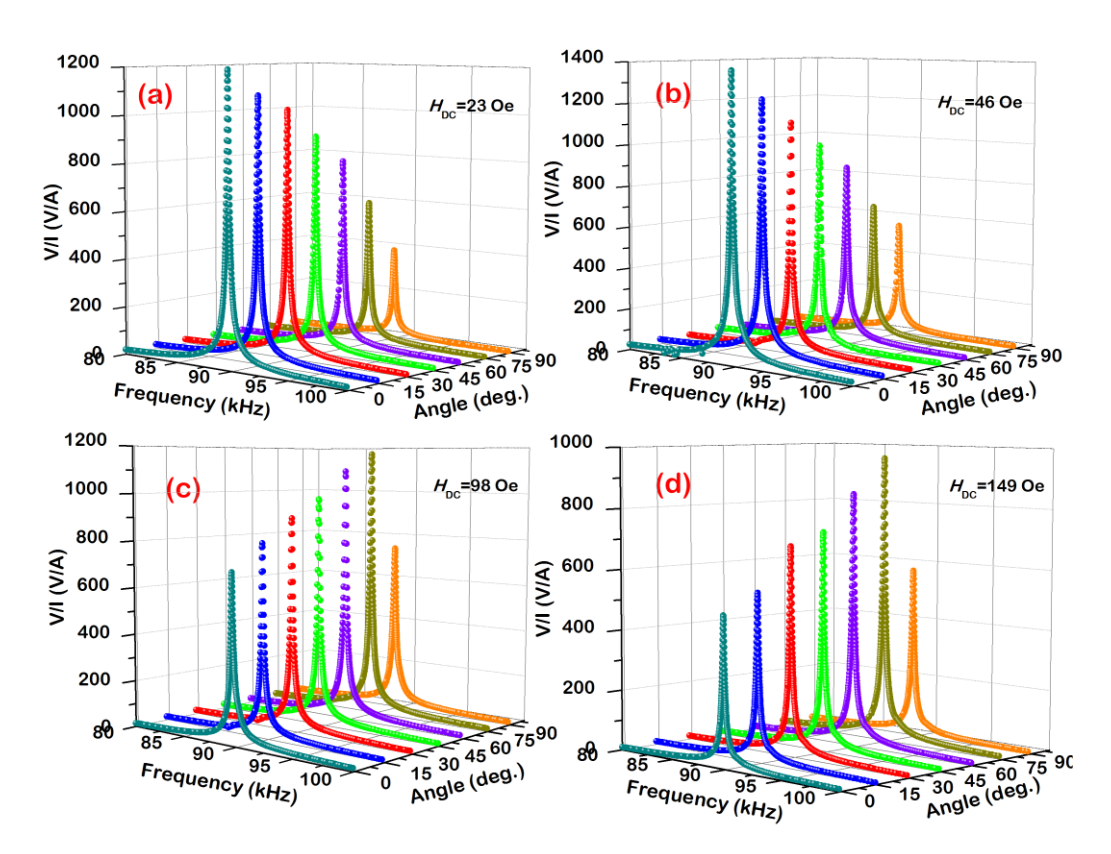


Fig 7. *I-V* ratios around resonance for θ varied from 0° to 90° under (a) H_{DC} =23 Oe; (b) H_{DC} =46 Oe; (c) H_{DC} =98 Oe; H_{DC} =149 Oe

To further understand the direction of H_{DC} for the impact of I-V conversion ratio at resonance conditions, the I-V conversion ratios were measured and re-plotted in the range of θ =0°-360°, as shown in the polar coordinate diagram of Fig.8. Similarly, the I-V conversion ratios in polar coordinate diagram can also track the DMPC with θ varied from 0° to 360°. The I-V conversion ratio also shows an anisotropic behavior and distinct difference under a lower and saturation fields, the optimum θ for maximum I-V conversion ratio varied from 0° to 75° once the H_{DC} approaches its saturation state. Therefore, the I-V conversion ratio can also be improved by adjusting θ , especially the ME gyrator used in intensive magnetic field.

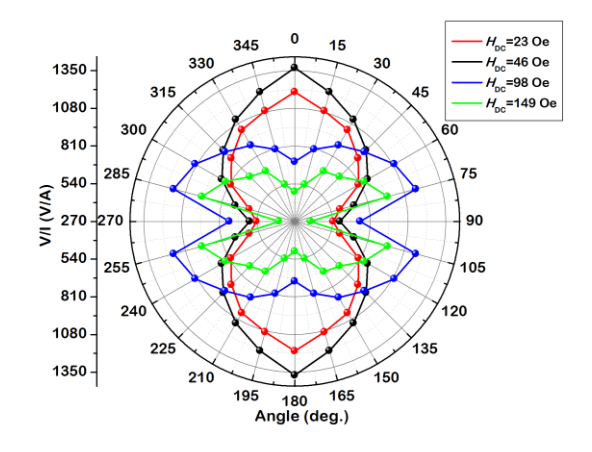


Fig 8. Polar diagram for resonance I-V ratios as a function of θ in the range of 0°-360° under

Generally, the ME composite and coil comprised the gyrators with two-port four-wire configuration to fulfill the conversion of inductance and capacitance or vice versa. In this scheme, coil port and piezoelectric port from ME composite in such ME gyrators can be considered as a medium to bridge inductive and capacitive networks for impedance matching etc. In view of this, measurements of inductance and impedance for coil port seem necessary. The coil is wound around the ME composite with dimensions of 45mm×10mm×5mm. The inductance and impedance for coil port were measured in the frequency range of 60-100kHz by an impedance analyzer to evaluate the required series resistance in input port (coil port) of ME gyrators, as shown in Fig 9(a). The inductance and impedance of $2.746\mu H$ and 11.8Ω were obtained at its inherent resonance frequency of 89kHz. In addition, the capacitance and impedance NZFO/PZT-8/NZFO laminate were investigated to characterize the capability of inductance to capacitance conversion and to estimate the required optimum resistance load for maximum power extraction. Figure 9(b) displayed the capacitance and impedance spectrum over 80-100kHz on symmetrical tri-layer NZFO/PZT-8/NZFO composite. Under the longitudinal acoustic working mode, the resonance and anti-resonance frequencies occurred at 89.0kHz and 89.6kHz, respectively. Correspondingly, the impedance increases precipitously from 0.125 k Ω to 6.85 k Ω . It is noted that mechanical vibrating frequency is equal to the anti-resonance frequency, and similar reports were documented in previous works [39]. In addition, we find that the capacitance trace falls dramatically with lower damping effects from 2.64nF to -2.22nF in the vicinity of resonance. The result demonstrates that the feasibility of conversion from inductance to capacitance in ME gyrator at near EMR can be realized, and the performance of inductance of 2.746µH converts to capacitance of -2.22nF. The suppression of permittivity can account for this feasibility. As frequency varies from resonance to anti-resonance frequencies, the electric charges reduce in piezoelectric ceramics and it causes that the dipole alignment reduction, and thus ε was suppressed[40]. The well-matched resistance load could be calculated to estimate anti-resonance impedance for the sake of maximizing power.

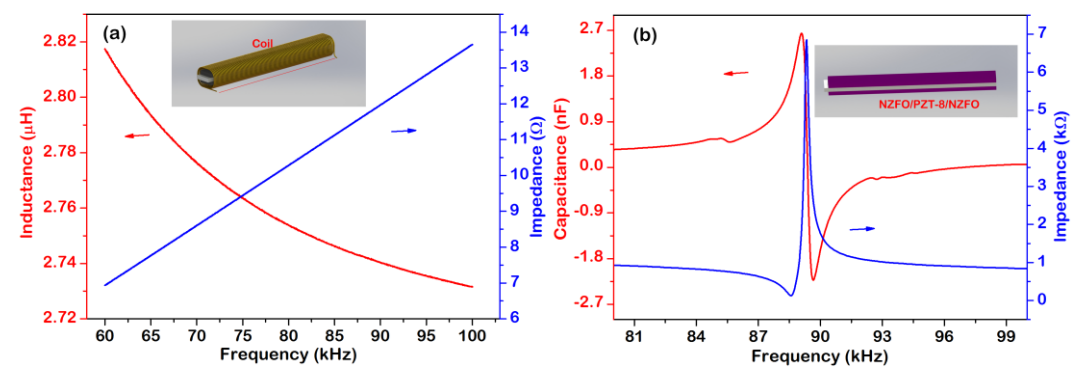


Fig 9. (a) The inductance and impedance spectrum in coil port were measured over 60-100kHz; (b) The capacitance and impedance spectrum of the ME port were measured over 80-100kHz.

Subsequently, the PE and output versus load resistance R were measured from 1Ω to $60k\Omega$ at zero magnetic fields as shown in Fig. 10(a). PE shows a dramatic rise

to its maximum of ~34.8% at R=6.7k Ω and then decreases with further increase in R, Simultaneously, the output voltage approaches to its saturation state and stabilizes at R=6.7k Ω with value of 1066.7 mV. Accordingly, the experimental results of H_{DC} dependence of PE at optimum load resistance and resonance for various θ as shown in Fig 10 (b). The PE in ME gyrator with tri-layered NZFO/PZT-8/NZFO and coil for each θ shows a rise followed by a decrease with the increase in H_{DC} , while the peak of PE and its corresponding optimum magnitude of H_{DC} display a shifting within the whole range. To be specific, the maximum of 80.3% in PE is obtained at θ =0° under H_{DC} =46 Oe. Once the H_{DC} exceeds 46 Oe the maximum peak, a maximum of ~76.5% corresponds to optimum θ =75°. The anisotropic dynamic magneto-elastic variation caused by demagnetization and magnetic domain rotation via θ rotations are responsible for the anisotropic PE behaviors.

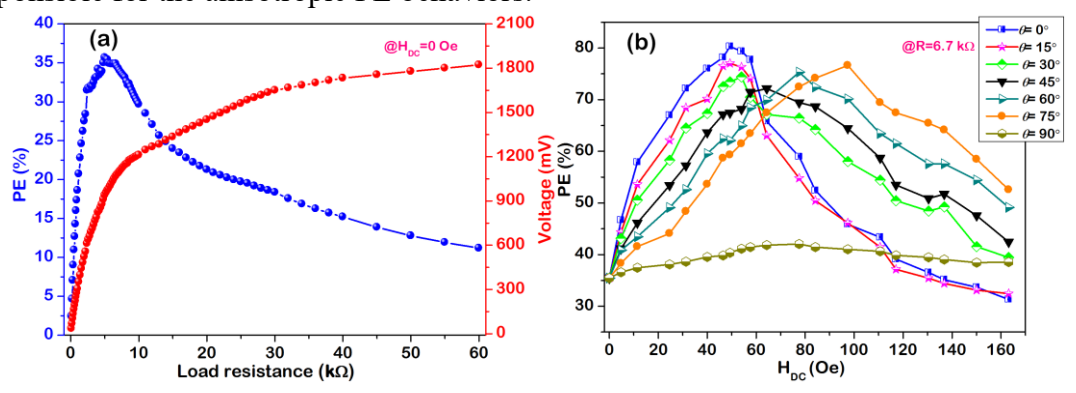


Fig.10 (a) PE and output voltage versus load resistance for the presented ME gyrator at H_{DC} =0; (b) PE as a function of H_{DC} for various typical θ at optimum load resistance.

In order to give a clear insight for the PE vs θ variations, the PE in ME gyrators under several typical H_{DC} (23Oe, 46Oe, 98Oe and 149 Oe) were re-plotted in Fig 11. PE vs θ profile also shows anisotropic behaviors in polar coordinate diagram, and tracks the I-V conversion ratio vs θ profile and the DPMC vs θ under various H_{DC} properly. As H_{DC} is increased from 23Oe to 149 Oe, the evolution of θ dependence of PE initially shows a typical twofold symmetry at 23Oe and then increases, followed with 'butterfly-like' fourfold symmetry and finally shrinks at 149 Oe. In other words, the maximum PE in ME gyrator was observed at θ =0° and 180° in lower magnetic field, whereas maximum PE in ME gyrator was found at θ =75°, 105°, 225° and 285° in saturation magnetic field. Obviously, there is an enhancement in PE observed at non-zero angle for saturation field, which is far higher than that at zero angle. These results provide an efficient methodology to improve PE for ME gyrator enabling it to work in external magnetic field situations. The stability of PE in ME gyrator for θ =0° and 75° under H_{DC} =98 Oe were measured input power density of 40 mW/cm³ as illustrated in Fig. 11(b). Experiment results show that a favorable stability of ME gyrator for two θ states in a higher magnetic field, and the PE at θ =75° (~76.5%) is 1.69 times higher than that of $\theta=0^{\circ}$ (~47.6%). Thus, a feasible approach introduced by means of θ rotations to fulfill efficient anisotropic magneto-elastic conversion as well as PE in ME gyrator.

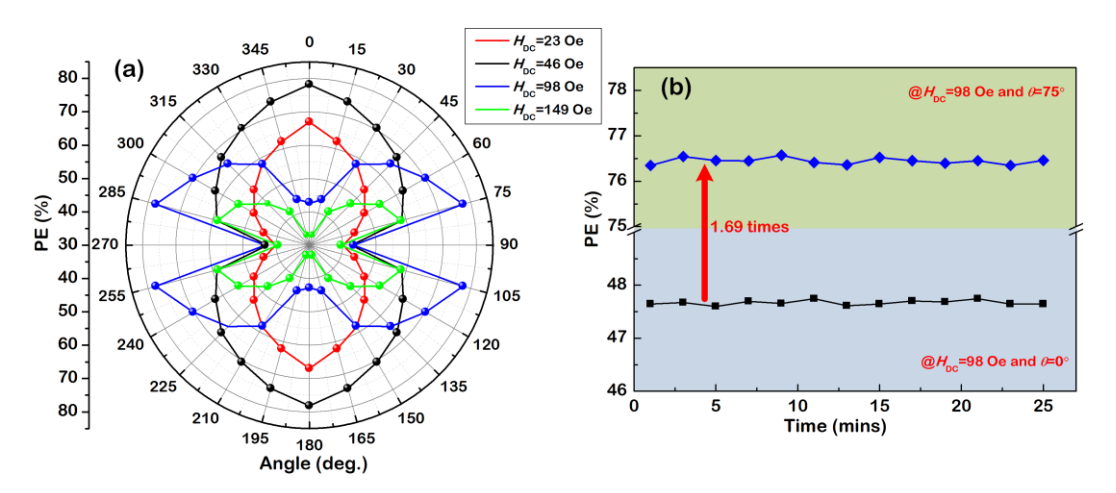


Fig.11 (a) Polar diagram of PE and output voltage vs load resistance for ME gyrator at H_{DC} =0; (b) the PE stability for θ =0° and 75° under H_{DC} =980e in high power density of 40mW/cm³.

IV. Conclusion

In summary, an effective methodology was introduced for further improvement of PE in tri-layer ferrite/PZT/ferrite ME-coil gyrators. Taking advantage of the anisotropic magneto-elastic variations aroused from the direction of applied $H_{\rm DC}$ rotating, enhanced ME couplings as well as PE was achieved under a certain angle with maximum effective magnetic field applied. From the simulation and experiment results, major findings were summarized as the following bullet points: (i) I-V vs θ and PE vs θ data can essentially track the DPMC vs θ profile, which means that the $H_{\rm DC}$ rotation induced anisotropic magneto-elastic variations are responsible for the eventual PE improvement. (ii) As θ is rotated from 0° to 360° with increment of 30°, PE vs θ profile polar diagram shows an anisotropic behavior response with a twofold symmetrical profile at lower field while a 'butterfly-like' fourfold symmetrical one at saturation field, and maximum in PE reaches ~80.3\% and ~76.5\% for θ =0\cdot\ in H_{DC} =46Oe and θ =75° at H_{DC} = 98Oe, respectively. (iii) Under higher magnetic field application, PE at θ =75° (~76.5%) shows 1.69 times higher than that of θ =0° (~47.6%) under input power density of 40mW/cm³ with favorable stabilities. These findings provide efficient methodology, and experimental evidence for further PE improvement with enhanced flexibility of the ME gyrator design.

Acknowledgements

This research was financially supported by National Natural Science Foundation of China (NSFC) (Grant Nos. 61973279, 62004177, 62073299), Program for Innovative Research Group (in Science and Technology) in University of Henan Province (No.20IRTSTHN017). The study at Russia was supported by the Russian Foundation for Basic Research (Grant No. 18-52-00021). The research at Oakland University was supported by a grant from the National Science Foundation (Grant No. DMR-1808892).

References

- [1] B. Tellegen, Philips. Res, 3 (1948) 81.
- [2] X. Zhuang, C. M. Leung, J. Fan, G. Srinivasan, D. Viehland, IEEE Trans. Ind. Electron, 66 (2019) 2499-2505.
- [3] X. Zhuang, C.M. Leung, J. Li, G. Srinivasan, D. Viehland, IEEE Trans. Ind. Electron, 66 (2018) 2499.
- [4] C.M. Leung, G. Sreenivasulu, X. Zhuang, X. Tang, M. Gao, J.R. Xu, J.F. Li, J.T. Zhang, G. Srinivasan, D. Viehland, Phys. Status. Solid: R, 12 (2018) 1800043.
- [5] K. Li, J.T. Zhang, Q.F. Zhang, D.A. Filippov, J. Wu, J.G. Tao, L.Y. Jiang, L.Z. Cao, G. Srinivasan, J. Mater. Sci: Mater. El, 32 (2021) 2249-2257.
- [6] Z.Q. Chu, M. PourhosseiniAsl, S.X. Dong, J. Phys. D: Appl. Phys, 51 (2018) 243001.
- [7] M.I. Bichurin, D. Viehland, G. Srinivasan, J. Electroceram, 19 (2007) 243-250.
- [8] N.A. Spaldin, R. Ramesh, Nat. mater, 18 (2019) 203-212.
- [9] J.T. Zhang, D.Y. Chen, D.A. Filippov, K. Li, Q.F. Zhang, L.Y. Jiang, W.W. Zhu, L.Z. Cao, G. Srinivasan, Appl. Phys. Lett, 113 (2018) 113502.
- [10] J.T. Zhang, D.Y. Chen, K. Li, D.A. Filippov, B.F. Ge, Q.F. Zhang, X.X. Hang, L.Z. Cao, G. Srinivasan, AIP Adv, 9 (2019) 035137.
- [11] J.T. Zhang, B.F. Ge, Q.F. Zhang, D.A. Filippov, J. Wu, J.G. Tao, Z.C. Jia, L.Y. Jiang, L.Z. Cao, G. Srinivasan, Appl. Phys. Lett, 118 (2021) 042402.
- [12] J.Y. Zhai, J.F. Li, S.X. Dong, D. Viehland, M.I. Bichurin, J. Appl. Phys, 100 (2006) 81.
- [13] J.Y. Zhai, J.F. Gao, C. De. Vreugd, J. Li, D. Viehland, A.V. Filippov, M.I. Bichurin, D.V. Drozdov, G.A. Semenov, S.X. Dong, Eur. Phys. J. B, 71 (2009) 383-385.
- [14] C.M. Leung, X. Zhuang, J.R. Xu, G. Srinivasan, J.F. Li, D. Viehland, Appl. Phys. Lett, 109 (2016) 202907.
- [15] C.M. Leung, X. Zhuang, D. Friedrichs, J.F. Li, R.W. Erickson, V. Laletin, M. Popov, G. Srinivasan, D. Viehland, Appl. Phys. Lett, 111 (2017) 122904.
- [16] C.M. Leung, X. Zhuang, M. Gao, X. Tang, J.R. Xu, J.F. Li, J.T. Zhang, G. Srinivasan, D. Viehland, Appl. Phys. Lett, 111 (2017) 182901.
- [17] X. Zhuang, C.M. Leung, J. Li, D. Viehland, Appl. Phys. Lett, 111 (2017) 103902.
- [18] C.M. Leung, X. Zhuang, J.R. Xu, J.F. Li, G. Srinivasan, D. Viehland, Appl. Phys. Lett, 110 (2017) 112904.
- [19] C.M. Leung, G. Sreenivasulu, X. Zhuang, M. Gao, X. Tang, J.R. Xu, J.F. Li, G. Srinivasan, D. Viehland, Appl. Phys. Lett, 112 (2018) 242901.
- [20] J.T. Zhang, W.W. Zhu, D.A. Filippov, W. He, D.Y. Chen, K. Li, S.T. Geng, Q.F. Zhang, L.Y. Jiang, L.Z. Cao, R. Timilsina, G. Srinivasan, Rev. Sci. Instrum, 90 (2019) 015004.
- [21] X. Zhuang, C.M. Leung, J.F. Li, G. Srinivasan, D. Viehland, IEEE Trans. Ind. Electron, 66 (2019) 2499-2505.
- [22] J.T. Zhang, W.W. Zhu, D.Y. Chen, H.W. Qu, P. Zhou, M. Popov, L.Y. Jiang, L.Z. Cao, G. Srinivasan, J. Magn. Magn. Mater, 473 (2019) 131-135.
- [23] C.M. Leung, X. Zhuang, J.R. Xu, M. Gao, X. Tang, J.F. Li, P. Zhou, G. Srinivasan, D. Viehland, J. Phys. D: Appl. Phys, 52 (2019) 065003.
- [24] C.M. Leung, J.R. Xu, X. Tang, M. Gao, J.F. Li, D. Viehland, IEEE Trans. Ind. Electron, 68 (2021) 1646-1653.

- [25] Y. Zong, Z. Yue, M.J. Higgins, Macromol. Mater. Mng, 308 (2018) 1800099.
- [26] X. Zhuang, C. Dolabdjian, C.M. Leung, J. Xu, D. Viehland, Sensor. Actuat. A: Phys, 302 (2019) 111815.
- [27] J.T. Zhang, J.H. Liu, Q.F. Zhang, D.A. Filippov, K. Li, J. Wu, J.G. Tao, L.Y. Jiang, L.Z. Cao, G. Srinivasan, Rev. Sci. Instrum, 92 (2021) 045006.
- [28] J.T. Zhang, K. Li, D.Y. Chen, D.A. Filippov, Q.F. Zhang, S.Y. Li, X. Peng, J. Wu, R. Timilsina, L.Z. Cao, G. Srinivasan, J. Electron. Mater, 49 (2020) 1120-1130.
- [29] A. Aubert, V. Loyau, G. Chaplier, F. Mazaleyrat, M. Lobue, J Mater Sc.: Mater El, 29 (2018) 14435–14444.
- [30] L. Niu, Y. Shi, Y. Gao, AIP Adv, 9 (2019) 045216.
- [31] L.Z. Cao, D.Y. Chen, S.T. Geng, Q.F. Zhang, K. Li, X.X. Hang, B.F. Ge, J.H. Liu, Y. Ruan, R. Timilsina, L.Y. Jiang, J.T. Zhang, J. Mater. Sci: Mater. El, 30 (2019) 16347-16352.
- [32] S. Chen, X. Yang, J. Ouyang, G. Lin, F. Jin, B. Tong, Ceram. Int, 40 (2014) 3419-3423.
- [33] J.T. Zhang, H.W. Zhao, Q.F. Zhang, A. Filippo, J. Wu, J.G. Tao, L.Y. Jiang, L.Z. Cao, G. Srinivasan, J. Magn. Magn. Mater, 524 (2021) 167680
- [34] J.T. Zhang, K. Li, D.Y. Chen, D.A. Filippov, Q.F. Zhang, J. Wu, J.G. Tao, L.Z. Cao, G. Srinivasan, J. Magn. Magn. Mater, 494 (2020).
- [35] H. Yao, Y. Shi, Y.W. Gao, J. Appl. Phys, 118 (2015) 234104.
- [36] C.S. Zhang, T.Y. Ma, M. Yan, J. Appl. Phys, 110 (2011) 063901.
- [37] W.G. Yang, N.A. Morley, J. Sharp, T. Ye, W.M. Rainforth, Appl. Phys. Lett, 108 (2016) 93.
- [38] T.X. Nan, Z.Y. Zhou, M. Liu, X. Yang, Y. Gao, B.A. Assaf, H. Lin, S. Velu, X.J. Wang, H.S. Luo, J. Chen, S. Akhtar, E. Hu, R. Rajiv, K. Krishnan, S. Sreedhar, D. Heiman, B.M. Howe, G.J. Brown, N.X. Sun, Sci. Rep-Uk, 4 (2014) 3688.
- [39] Z. Wu, Z.H. Xiang, Y.M. Jia, Y.H. Zhang, H.S. Luo, J. Appl. Phys, 112 (2012) 106102
- [40] L.H. Chen, J.B. Guo, X. Wang, X.W. Dong, H.X. Zhao, L.S. Long, L.S. Zheng, Adv. Mater, 29 (2017) 1702512.